An effective model for the $X\,^2A_1-A\,^2B_2$ conical intersection in NO_2

M. Joyeux,[a] R. Jost, and M. Lombardi
Laboratoire de Spectrométrie Physique (CNRS UMR 5588), Université Joseph Fourier-Grenoble 1, BP 87, 38402 St. Martin d'Hères Cedex, France

(Received 14 May 2003; accepted 25 June 2003)

We propose an efficient method for calculating the eigenstates and adjusting the parameters of an effective Hamiltonian, which reproduces the experimentally observed energy levels of NO_2 up to 11 800 cm^{-1} above the quantum mechanical ground state, that is a few thousands of cm^{-1} above the $X\,^2A_1-A\,^2B_2$ conical intersection, with a rms error less than 4 cm^{-1}. This method principally relies on the determination, through first-order perturbation theory, of an optimal basis for each surface, which takes into account the nonresonant energy shifts experienced by the states of this surface. As a result, the size of the matrix, which one has to build and diagonalize to converge the spectrum up to 11 800 cm^{-1}, is of the order of 500–1000 instead of several tens of thousands. Thank to this Hamiltonian, the analysis of the experimental spectrum up to 11 800 cm^{-1} could be completed. A detailed description of all states located above 9500 cm^{-1} is proposed, those lying below 9500 cm^{-1} being already known and tabulated. © *2003 American Institute of Physics.*
[DOI: 10.1063/1.1601602]

I. INTRODUCTION

The Born–Oppenheimer separation of electronic and nuclear motions is a widely used approximation for interpreting molecular processes. Nonetheless, transitions between different electronic surfaces (non-Born–Oppenheimer, or nonadiabatic, dynamics) represent a field of growing interest in chemical physics, because they appear to govern a large variety of fundamental processes, such as internal conversion, intersystem crossing, electron transfer and photoinduced reactions. In this context, the conical intersection between the two lowest electronic surfaces of NO_2, $X\,^2A_1$ and $A\,^2B_2$, has already attracted much attention from both the experimental (see Refs. 1–4, and references therein) and theoretical (see Refs. 5–13, and references therein) points of view. However, there still exists no model that satisfactorily reproduces the vibronic spectrum of NO_2 in the region of the conical intersection, i.e., around 10 000 cm^{-1}. We recently made an attempt in this direction, by adjusting the parameters of a diabatic effective Hamiltonian against the energies of the lowest 283 vibronic states, which have now all been observed experimentally.[14] The associated vibronic states, which extend up to 11 400 cm^{-1} above the quantum mechanical ground state, consist of 276 states with predominant $X\,^2A_1$ ground electronic character and 7 states with predominant $A\,^2B_2$ excited electronic character. These calculations were based on the observation, that the net effect of the diabatic coupling between the two surfaces can be divided into two contributions, namely (i) a nonresonant coupling, which affects all of the $X\,^2A_1$ vibrational states but is associated to very weak mixing coefficients and (ii) a resonant coupling, which is significant (below 11 400 cm^{-1}) for only few $X\,^2A_1$ states, but induces a significant mixing of these states with one (or few) energetically close $A\,^2B_2$ state(s).[15,16]

The results obtained in this first work are perfectible in several ways. First, no effective Hamiltonian could be derived for the $A\,^2B_2$ excited electronic surface, because we did not calculate the energy shifts experienced by the states of this surface following the nonresonant couplings with the states of the ground electronic surface. Therefore, the excited electronic surface was rather described as a list of discrete energies. Moreover, the calculation procedure was rather approximate, since only very small matrices, corresponding to the resonantly coupled states of both electronic surfaces, were diagonalized. At last, the overlap matrix elements used in this first work were not precise enough, because of the loss of an unexpectedly large number of accuracy digits (several tens of them) following near cancellation of very large numbers.

The purpose of the present article is to report on the derivation of a complete effective Hamiltonian based on numerically exact quantum calculations. In this model, two Dunham expansions are used to describe, respectively, the uncoupled ground and excited diabatic electronic surfaces. The effective Hamiltonian for the ground electronic surface additionally includes a weak vibrational resonance. The third component of the effective Hamiltonian, i.e., the diabatic coupling surface, is taken as the usual λq_3 interaction, where q_3 is the antisymmetric stretch normal coordinate for the electronic ground surface. When adjusting the parameters of such a model against experimental data, the main concern deals with CPU time, that is, in other terms, the size of the Hamiltonian matrix one has to build and diagonalize. Since λ is of the order of several hundreds of cm^{-1}, the diabatic coupling between states separated by several tens of thousands of cm^{-1} still has a sizable effect on the energy of each state. Moreover, each state is coupled to several tens of thou-

[a]Author to whom correspondence should be addressed. Electronic mail: Marc.JOYEUX@ujf-grenoble.fr

sands of states belonging to the other surface and the resulting (nonresonant) energy shifts are cumulative. This explains why, when working with harmonic oscillator bases, the size of the Hamiltonian matrix, which is necessary to converge the spectrum up to 11 000 or 12 000 cm^{-1} above the ground state, is as large as several tens of thousands of vectors. These dimensions being not compatible with the large number of iterations required by an adjustment procedure, the work reported in this article principally relies on the choice of a different basis, which is obtained from first-order perturbation theory. It is however emphasized, that perturbation theory is used only to build the working basis, while the construction and diagonalization of the Hamiltonian matrix are numerically exact.

This point is explained in some detail in Sec. III. The effective Hamiltonian itself is described in Sec. II, while calculations and results are discussed in Sec. IV.

II. THE EFFECTIVE HAMILTONIAN

The effective diabatic Hamiltonian **H** is taken in the form,

$$\mathbf{H}=\begin{pmatrix} H_e & H_c \\ H_c & H_g \end{pmatrix}, \tag{2.1}$$

where H_g, H_e, and H_c describe the diabatic ground, excited and coupling surfaces, respectively. Let us note (p_1,q_1), (p_2,q_2), and (p_3,q_3) the sets of conjugate coordinates for, respectively, the symmetric stretching, the bending, and the antisymmetric stretching modes of vibration around the minimum of the $X\,^2A_1$ ground electronic surface, and $|v_1,v_2,v_3\rangle$ the direct product basis for these three harmonic oscillators. In this basis, H_g is taken as the sum of the eighth order Dunham expansion,

$$\begin{aligned}\langle v_1,v_2,v_3|H_g|v_1,v_2,v_3\rangle &= \sum_{i=1}^{3}\omega_i n_i+\sum_{i\leqslant j}x_{ij}n_in_j \\ &\quad+\sum_{i\leqslant j\leqslant k}y_{ijk}n_in_jn_k+\sum_{i\leqslant j\leqslant k\leqslant m}z_{ijkm}n_in_jn_kn_m,\end{aligned} \tag{2.2}$$

where $n_i=v_i+1/2$ $(i=1,2,3)$, plus the $3\omega_1\approx\omega_2+2\omega_3$ vibrational resonance,

$$\begin{aligned}\langle v_1,v_2,v_3|H_g|v_1-3,v_2+1,v_3+2\rangle &= \left(k+\sum_{i=1}^{3}k_in_i\right) \\ &\quad\times\sqrt{v_1(v_1-1)(v_1-2)(v_2+1)(v_3+1)(v_3+2)},\end{aligned} \tag{2.3}$$

where $n_1=v_1-1$, $n_2=v_2+1$, and $n_3=v_3+3/2$. Let us similarly note (p_1',q_1'), (p_2',q_2'), and (p_3',q_3') the sets of conjugate coordinates for, respectively, the symmetric stretching, the bending and the antisymmetric stretching modes of vibration around the minimum of the $A\,^2B_2$ excited electronic surface, and $|v_1',v_2',v_3'\rangle$ the direct product basis for these three harmonic oscillators. The experimental data for the excited surface being much sparser than for the ground one, H_e is taken to be just the energy difference between the bottoms of the two electronic surfaces plus a fourth order Dunham expansion,

$$\begin{aligned}\langle v_1',v_2',v_3'|H_e|v_1',v_2',v_3'\rangle &= E_0'+\sum_{i=1}^{3}\omega_i'n_i'+\sum_{i\leqslant j}x_{ij}'n_i'n_j',\end{aligned} \tag{2.4}$$

where $n_i'=v_i'+1/2$ $(i=1,2,3)$. At last, the diabatic coupling H_c is taken to be the only first-order term authorized by symmetry, that is

$$H_c=\lambda q_3. \tag{2.5}$$

Calculation of the $\langle v_1',v_2',v_3'|H_c|v_1,v_2,v_3\rangle$ integrals is *the* numerically difficult step in the process of building the full Hamiltonian matrix in the $|v_1,v_2,v_3\rangle$ and $|v_1',v_2',v_3'\rangle$ bases. In addition to the parameter λ, these integrals depend only on the relationship between the (q_1,q_2,q_3) and (q_1',q_2',q_3') sets of normal coordinates, which, as in Ref. 14, is taken in the form,

$$\begin{aligned}\begin{pmatrix} q_1' \\ q_2' \\ q_3' \end{pmatrix} &= \mathbf{A}\begin{pmatrix} q_1 \\ q_2 \\ q_3 \end{pmatrix}+\mathbf{B} \\ &= \begin{pmatrix} 0.899 & -0.532 & 0 \\ 0.301 & 0.906 & 0 \\ 0 & 0 & 0.693 \end{pmatrix}\begin{pmatrix} q_1 \\ q_2 \\ q_3 \end{pmatrix}+\begin{pmatrix} 1.100 \\ -5.730 \\ 0 \end{pmatrix}.\end{aligned} \tag{2.6}$$

This relationship was kept fixed in all of our calculations, although the fundamental frequencies were allowed to vary slightly around the values, which were used to obtain Eq. (2.6). This is of little practical consequence, because the equilibrium geometry of the excited surface is anyway still rather poorly known.[4] Since the numerical calculation of these integrals is one of the fundamental issues for this study, the procedure we used to calculate them is sketched in the Appendix.

As already noted in the Introduction, the principal problem, which arises when using Eqs. (2.1)–(2.6) to build and diagonalize the Hamiltonian matrix, is the size of the total harmonic basis. Indeed, this basis must contain several tens of thousands of vectors if the spectrum is to be converged up to 11 000 or 12 000 cm^{-1} above the quantum mechanical ground state. This size being not compatible with the large number of iterations required by an adjustment procedure, we had to work with a more suitable basis, obtained from first order perturbation theory. The procedure for determining this basis, as well as the calculation of the matrix elements of **H** in the new basis, are described in some detail in the following section.

III. THE PERTURBATIVE BASIS

Let us note E_n^g and E_n^e the eigenvalues of the uncoupled Hamiltonians H_g and H_e and φ_n^g and φ_n^e the associated eigenvectors,

$$H_g\varphi_n^g=E_n^g\varphi_n^g,$$
$$H_e\varphi_n^e=E_n^e\varphi_n^e. \tag{3.1}$$

The eigenvectors of the full Hamiltonian **H** of Eq. (2.1) are obtained, at first order of perturbation theory, in the form

$$\begin{pmatrix} \sum_k \dfrac{\langle\varphi_k^e|H_c|\varphi_n^g\rangle}{E_n^g-E_k^e}\varphi_k^e \\ \varphi_n^g \end{pmatrix}, \tag{3.2}$$

for the eigenvectors of **H** built on the eigenvectors of H_g, and

$$\begin{pmatrix} \varphi_n^e \\ \sum_k \dfrac{\langle\varphi_n^e|H_c|\varphi_k^g\rangle}{E_n^e-E_k^g}\varphi_k^g \end{pmatrix} \tag{3.3}$$

for those built on the eigenvectors of H_e. It is well-known, that the vectors in Eqs. (3.2)–(3.3) are good approximations of the eigenvectors of **H** if (and only if) the ratios which appear in these equations remain small, that is, if the zero-order energies E_n^g of the ground electronic surface are not accidentally close to the zero-order energies E_n^e of the excited electronic surface. If this condition is not fulfilled, that is, if there exist accidental resonances between specific pairs of states belonging to different electronic surfaces, then the approximation breaks down. It is therefore interesting to build new bases of vectors ψ_n^g and ψ_n^e, such that

$$\psi_n^g=\begin{pmatrix} \sum_k \alpha_{nk}\varphi_k^e \\ \varphi_n^g \end{pmatrix}, \quad \psi_n^e=\begin{pmatrix} \varphi_n^e \\ \sum_k \beta_{nk}\varphi_k^g \end{pmatrix}, \tag{3.4}$$

where the coefficients α_{nk} and β_{nk} are defined as follows:

$$\text{if } \left|\frac{\langle\varphi_k^e|H_c|\varphi_n^g\rangle}{E_n^g-E_k^e}\right|\leqslant\varepsilon,$$
$$\text{then } \alpha_{nk}=\frac{\langle\varphi_k^e|H_c|\varphi_n^g\rangle}{E_n^g-E_k^e} \text{ else } \alpha_{nk}=0,$$
$$\text{if } \left|\frac{\langle\varphi_n^e|H_c|\varphi_k^g\rangle}{E_n^e-E_k^g}\right|\leqslant\varepsilon,$$
$$\text{then } \beta_{nk}=\frac{\langle\varphi_n^e|H_c|\varphi_k^g\rangle}{E_n^e-E_k^g} \text{ else } \beta_{nk}=0. \tag{3.5}$$

In Eq. (3.5), ε is a threshold parameter, which separates resonantly (large ratios) from nonresonantly (small ratios) coupled pairs of zero-order eigenstates. We used $\varepsilon=0.05$ in the calculations reported in this article but, of course, the final result does not depend on the precise value of ε. The matrix elements of **H** in the new basis are next obtained in the form,

$$\begin{aligned}
\langle\psi_m^g|\mathbf{H}|\psi_n^g\rangle &= \delta_{mn}E_n^g+\sum_k\,(\alpha_{mk}\alpha_{nk}E_k^e+\alpha_{mk}\langle\varphi_k^e|H_c|\varphi_n^g\rangle \\
&\quad +\alpha_{nk}\langle\varphi_k^e|H_c|\varphi_m^g\rangle), \\
\langle\psi_m^e|\mathbf{H}|\psi_n^e\rangle &= \delta_{mn}E_n^e+\sum_k\,(\beta_{mk}\beta_{nk}E_k^g+\beta_{mk}\langle\varphi_n^e|H_c|\varphi_k^g\rangle \\
&\quad +\beta_{nk}\langle\varphi_m^e|H_c|\varphi_k^g\rangle), \\
\langle\psi_m^e|\mathbf{H}|\psi_n^g\rangle &= \langle\varphi_m^e|H_c|\varphi_n^g\rangle+\alpha_{nm}E_m^e+\beta_{mn}E_n^g \\
&\quad +\sum_k\sum_j\,\alpha_{nj}\beta_{mk}\langle\varphi_j^e|H_c|\varphi_k^g\rangle,
\end{aligned} \tag{3.6}$$

where δ_{mn} is Kronecker's symbol. The last equation in Eq. (3.6) shows that, in the new basis of vectors ψ_n^g and ψ_n^e, the nonadiabatic coupling $\langle\psi_m^e|\mathbf{H}|\psi_n^g\rangle$ between two vectors belonging to different surfaces is small, except when the zero-order energies of these vectors are accidentally resonant. In this later case, the off-diagonal matrix element is close to the unperturbed one, that is to $\langle\varphi_m^e|H_c|\varphi_n^g\rangle$. Consequently, the size of the matrix one has to build to obtain a spectrum converged up to a given energy is of much smaller dimensions than the size required with the harmonic basis. For example, this size is typically of the order of 500–1000 to converge the spectrum up to 11 800 cm^{-1}.

Before concluding this section, it is perhaps not completely useless to emphasize that the basis defined by Eqs. (3.4)–(3.5) is neither orthogonal nor normalized, so that the energy levels and the quantum states of **H** are *not* obtained as the eigenvalues and eigenvectors of the Hamiltonian matrix computed in this basis. In the perturbative basis, one has instead to solve the slightly more complex generalized eigenproblem,

$$\mathbf{H}\psi=E\mathbf{N}\psi, \tag{3.7}$$

where **N** is the matrix of the overlaps $\langle\psi_m^g|\psi_n^g\rangle$, $\langle\psi_m^e|\psi_n^e\rangle$, and $\langle\psi_m^e|\psi_n^g\rangle$ (**N** is equal to the identity matrix in the case of an orthonormalized basis). A numerically efficient method for solving Eq. (3.7) consists in finding the matrices **V** and $\mathbf{\Lambda}$ of, respectively, the eigenvectors and eigenvalues of **N**,

$$\mathbf{NV}=\mathbf{V\Lambda} \tag{3.8}$$

and in calculating the matrix **M**,

$$\mathbf{M}=\mathbf{V\Lambda}^{-1/2\,t}\mathbf{V} \tag{3.9}$$

(**M** is also equal to the identity matrix in the case of an orthonormalized basis). Simple calculations then show that the quantized energies of Eq. (3.7) are the eigenvalues of **M H M**, while the matrix of the generalized eigenvectors of Eq. (3.7) is equal to the matrix of the eigenvectors of **M H M** multiplied, on the left-hand side, by **M**.

IV. CALCULATIONS, RESULTS, AND DISCUSSION

To summarize, actual calculations are performed as follows. The initial basis is first determined by retaining all the vectors $|v_1,v_2,v_3\rangle$ and $|v_1',v_2',v_3'\rangle$, such that

$$1337v_1+758v_2+1672v_3\leqslant E^g_{\max},$$
$$9700+1310v'_1+745v'_2+800v'_3\leqslant E^e_{\max}. \tag{4.1}$$

For the purpose of calculating the spectrum up to 11 800 cm^{-1} above the quantum mechanical ground state, suitable values for the upper limits are $E^g_{\max}=30\,000\ cm^{-1}$ and $E^e_{\max}=50\,000\ cm^{-1}$, which leads to basis sizes of 3182 and 15 504 for, respectively, the ground and excited surfaces.

The eigenstates of the uncoupled Hamiltonians H_g and H_e are then evaluated for each new set of parameters of the effective Hamiltonian. The eigenvectors φ^e_n of H_e are obviously just the $|v'_1,v'_2,v'_3\rangle$ vectors, while the corresponding eigenvalues E^e_n are calculated according to Eq. (2.4). In contrast, calculation of the functions φ^g_n and the energies E^g_n for the ground electronic surface requires some more effort, since these quantities are obtained from the diagonalization of small matrices of $|v_1,v_2,v_3\rangle$ vectors coupled by the $3\omega_1\approx\omega_2+2\omega_3$ resonance of Eq. (2.3).

The perturbative basis, which consists of the vectors ψ^g_n and ψ^e_n of Eqs. (3.4)–(3.5), is next evaluated. One retains in this basis all the vectors ψ^g_n and ψ^e_n, which are built on vectors φ^g_n and φ^e_n with associated zero-order energies E^g_n and E^e_n smaller than a given threshold $E_{\max}$ (relative to the minimum of the ground electronic surface). In order to check the convergence of the calculations, the results obtained with two different values of $E_{\max}$ are compared, namely, $E_{\max}=16\,000\ cm^{-1}$ (about 500 vectors for the ground surface and 40 vectors for the excited surface) and $E_{\max}=20\,000\ cm^{-1}$ (about 1200 vectors for the ground surface and 200 vectors for the excited surface). Note that, according to Eqs. (3.4)–(3.5), each vector ψ^g_n depends, in addition to φ^g_n, on the 15 504 vectors $|v'_1,v'_2,v'_3\rangle$, while each vector ψ^e_n depends, in addition to φ^e_n, on the 3182 vectors $|v_1,v_2,v_3\rangle$.

At last, the Hamiltonian matrix is built according to Eq. (3.6) and the quantized states of **H** are obtained from the procedure sketched at the end of Sec. III. Eventually, the eigenvectors of **H** are expressed back in terms of the vectors $|v_1,v_2,v_3\rangle$ and $|v'_1,v'_2,v'_3\rangle$. After comparison of the calculated and experimental spectra, the standard gradient method is used to minimize the computed root-mean-square (rms) error.

The experimental spectrum up to 11 800 cm^{-1} above the quantum mechanical ground state (against 11 400 cm^{-1} in Ref. 14) was used to adjust the parameters of the effective Hamiltonian. This energy window contains 298 states with predominant $X\,^2A_1$ ground electronic character and nine states with predominant $A\,^2B_2$ excited electronic character, of which only 1 state with predominant $A\,^2B_2$ excited electronic character ([1,0,1]) has not been observed experimentally. In addition to energy, the experimental spectrum also provides a clear-cut determination of the total *vibronic* symmetry (A_1 or B_2) of the recorded states.[1–4] The vibrational terms (i.e., the rotationless band origins) of states with A_1 vibronic symmetry are directly obtained from the recorded laser induced dispersed fluorescence (LIDFS) spectra. In contrast, the lowest rotational level of states with B_2 vibronic symmetry observed in LIDFS spectra is $N=K=1$. For the purpose of comparison with calculated energies, these observed energies are extrapolated down to $N=K=0$ by subtracting from the observed energies the rotational constant $A+\overline{B}$, where A and $\overline{B}$ are estimated according to Eqs. (1) and (2) of Ref. 3.

TABLE I. Adjusted values (second column) and standard deviations (third column) for the parameters of the effective Hamiltonian of Eqs. (2.1)–(2.6). All values are expressed in cm^{-1}.

	Value	Uncertainty
ω_1	1357.4090	3.2911
ω_2	756.8245	0.8396
ω_3	1670.3878	0.9327
x_{11}	−11.9870	1.5479
x_{12}	−5.0272	0.4345
x_{13}	−28.9949	0.2445
x_{22}	0.0763	0.1547
x_{23}	−10.4319	0.2975
x_{33}	−14.7341	0.1949
y_{111}	1.4238	0.2577
y_{112}	0.3033	0.1512
y_{122}	−0.2087	0.0226
y_{222}	−0.0363	0.0075
y_{233}	−0.1933	0.0477
z_{1111}	−0.0892	0.0137
z_{1112}	−0.0558	0.0148
z_{1113}	−0.2460	0.0071
z_{1123}	−0.1306	0.0230
z_{1223}	−0.0590	0.0162
z_{2233}	0.0186	0.0026
k	0.8360	0.1815
k_1	−0.1710	0.0561
E'_0	10 209.0874	20.2592
ω'_1	1315.0927	9.5659
ω'_2	766.2419	12.0323
ω'_3	753.1696	17.9987
x'_{12}	−36.9088	6.3631
x'_{23}	−43.3650	8.2839
x'_{33}	27.9314	4.6044
λ	331.7647	18.8067

A set of 30 converged parameters (22 parameters for H_g, 7 parameters for H_e, and 1 parameter for H_c) is shown in Table I. The rms and maximum errors between the measured energies and the calculated ones are 3.8 cm^{-1} and 19.7 cm^{-1}, respectively, for the 306 experimentally observed states. Fit residuals are plotted in Fig. 1(a) as a function of energy. Note that the small uncertainties reported in Table I for the parameters of H_e, as well as the small errors for the calculated energies of the eight states with predominant $A\,^2B_2$ excited electronic character, are largely meaningless since, for this surface, the number of parameters (7) is very close to the number of experimental data taken into account (8).

One of the most interesting information of Table I is the value for the coupling parameter $\lambda\approx 332\mp 19\ cm^{-1}$. The main reason, why this estimation is substantially smaller than the estimation of Ref. 14 ($\lambda\approx 600\ cm^{-1}$) is, as already stated in the Introduction, that the overlap matrix elements used in this first work were not precise enough, because of the loss of an unexpectedly large number of accuracy digits (several tens of them) following near cancellation of very large numbers. The overlap integrals were calculated to, roughly, only one half of their actual values, which resulted in an estima-

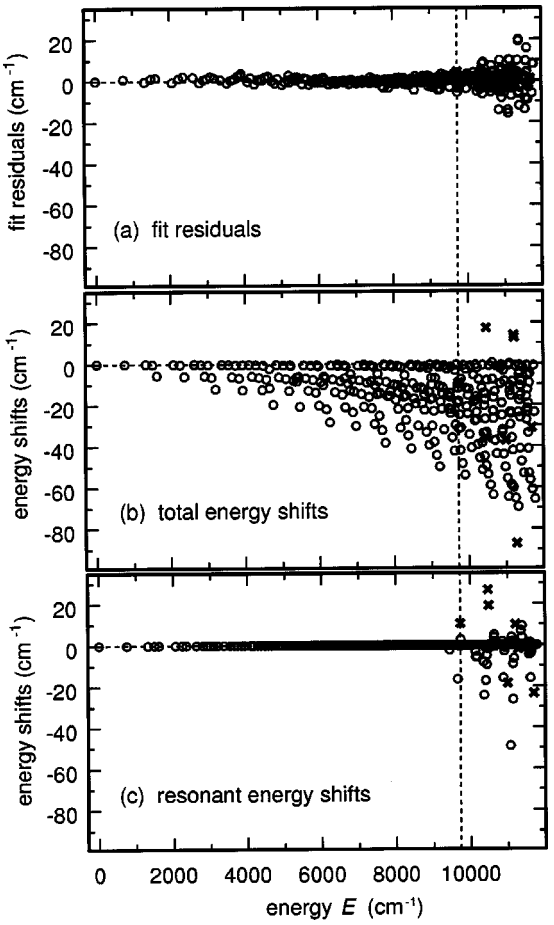

FIG. 1. (a) Plot of the fit residuals as a function of the experimentally determined energies up to 11 800 cm^{-1} above the quantum mechanical ground state. The fit residuals are defined as the difference between the experimentally determined energies and the eigenvalues of the effective Hamiltonian of Eqs. (2.1)–(2.6) and Table I. (b) Plot of the calculated total energy shifts caused by the diabatic coupling H_c as a function of the experimentally determined energies. The total energy shifts are defined as the difference between the eigenvalues of the effective Hamiltonian of Eqs. (2.1)–(2.6) and Table I and the eigenvalues obtained when setting $\lambda=0$. (c) Plot of the calculated resonant energy shifts caused by the diabatic coupling H_c as a function of the experimentally determined energies. The resonant energy shifts are defined as the difference between the eigenvalues of the effective Hamiltonian of Eqs. (2.1)–(2.6) and Table I and the eigenvalues obtained when setting all $\langle \psi_m^e|\mathbf{H}|\psi_n^g\rangle$ elements to zero in the Hamiltonian matrix expressed in the perturbative basis [a value $\varepsilon=0.05$ is assumed in the definitions of Eq. (3.5)]. In all plots, open circles denote states with predominant $X\ ^2A_1$ ground electronic character, while crosses ($\times$) denote states with predominant $A\ ^2B_2$ excited electronic character. The vertical lines indicate the energy of the vibrational ground state of the excited electronic surface. Note also that both the coordinate and abscissa scales are identical for the three plots.

tion for λ too large by a factor of about 2. It is stressed, once more, that the determination of λ does not rely on the total energy shifts caused by $H_c=\lambda q_3$, but only on a small part of these quantities, i.e., the resonant shifts. This point is clearly visualized in Figs. 1(b) and 1(c), which show, respectively, the total and resonant energy shifts caused by H_c. The total energy shifts of Fig. 1(b) are obtained by subtracting the energies calculated with $\lambda=0$ from the energies calculated with the parameters of Table I. Although this figure is somewhat obscured by the fact that the shifts for all of the states are displayed on the same plot, it is nevertheless clear that the largest part of these shifts increases regularly with quantum numbers and energy. We actually showed in Refs. 15 and 16 that the regular part of the energy shifts is due to the nonresonant couplings, that is, to the interactions between states of different surfaces, which are well separated in energy. We also showed that these nonresonant shifts cannot be distinguished from the anharmonicities inside each surface (hence the above remark that they are of no use for the determination of the coupling parameter λ). The principal reason, why the number of vectors required to converge the spectrum is much smaller with the perturbative basis of Sec. III than with the harmonic basis, is precisely that the perturbative basis for each surface takes into account, by construction, the nonresonant shifts experienced by the states of this surface. Therefore, the resonant shifts (i.e., the shifts resulting from the interaction between states of different surfaces which are almost degenerate in energy) can be obtained as the difference between the eigenvalues of the effective Hamiltonian of Eqs. (2.1)–(2.6) and the eigenvalues obtained when setting all $\langle \psi_m^e|\mathbf{H}|\psi_n^g\rangle$ elements to zero in the Hamiltonian matrix expressed in the perturbative basis. The result obtained with $\varepsilon=0.05$ is plotted in Fig. 1(c). It is seen that, in contrast with nonresonant ones, resonant shifts are significant only for a limited number of states. The present determination of λ actually relies on these (relatively few) resonant shifts and the resulting increase of precision in the calculated energies. It is therefore not excluded that this estimation for λ might still vary to some extent if the working data set is extended to higher energies. It turns out that the present estimation $\lambda\approx 332\mp 19\ cm^{-1}$ is of the same order of magnitude as the first experimental determination of Delon and Jost ($\lambda\approx 280\mp 50$) cm^{-1},[1] which was obtained from approximate calculations performed on a much more limited data set. In contrast, this value is much smaller than the estimations derived from recent *ab initio* calculations, which range from 700 cm^{-1} (Ref. 8) to more than 2400 cm^{-1}.[10] As stated in Ref. 8, the reason for such an uncertainty in the determination of λ is ''not clear at that point.''

This work and the previous one in Ref. 14 enable a better understanding of the experimental spectrum of NO_2 up to 11 800 cm^{-1} above the quantum mechanical ground state. Indeed, several states which were left unassigned in Table VI of Ref. 3 could be safely assigned in the course of this work, while some additional states could be retrieved in the recorded spectra thank to their calculated energies (this procedure eventually led to the reassignment of a few states). This is the first reason, why the energies of the states observed above 9500 cm^{-1} are reported in Table II together with their calculated decomposition on the harmonic oscillator bases. The description of states with lower energy can be found in Refs. 1 and 3. The second reason for reporting the computed eigenvectors in Table II is that, within the approximation of the effective Hamiltonian of Eqs. (2.1)–(2.6), the only important coupling observed below 9500 cm^{-1} is due to the approximate $3\omega_1\approx\omega_2+2\omega_3$ vibrational resonance of Eq. (2.3), while additional couplings due to H_c appear above 9500 cm^{-1}. Among these new couplings, the most important one is of course the resonant vibronic coupling between states of different surfaces, which gives rise to the resonant

TABLE II. NO_2 vibronic states located between 9500 and 11 800 cm^{-1} above the quantum mechanical ground state. The first column indicates the rank of the state in a given electronic surface (the quantum mechanical ground state of each surface is #1). The second column shows, for states with B_2 vibronic symmetry, the energy (in cm^{-1} above the quantum mechanical ground state) of the $N=K=1$ rotational component obtained from LIDFS experiments. The rotationless band origins are shown in the third column. For most states with B_2 vibronic symmetry, the band origin is obtained by subtracting the rotational constant $A+\overline{B}$ [estimated according to Eqs. (1) and (2) Ref. 3] from the $N=K=1$ energy reported in the second column. For states with A_1 vibronic symmetry, the energy of the band origin is directly obtained from LIDFS experiments. The fourth column indicates the difference between the ''experimental'' energy of column 3 and the energy obtained from the effective Hamiltonian of Eqs. (2.1)–(2.6) and the parameters of Table I. The fifth column shows the calculated probability (in percents) for finding the state in the diabatic excited electronic surface $A\,^2B_2$. A more precise description of the wave function is provided in the last column, which indicates its decomposition on the harmonic bases of the $X\,^2A_1$ (normal brackets) and $A\,^2B_2$ (square brackets) diabatic electronic surfaces. All calculated contributions larger than 0.1 are shown.

No.	Energy (cm^{-1}) $K=N=1$	Energy (cm^{-1}) $K=N=0$	obs.−calc. error (cm^{-1})	$\%A\,^2B_2$	Eigenvector decomposition
165	9510.20	9499.98	−0.08	0.16	0.715(1,5,3) − 0.697(4,4,1)
166		9512.15	0.26	0.02	0.979(4,2,2) − 0.199(1,3,4)
167	9529.28	9518.12	1.00	0.18	0.716(4,4,1) + 0.695(1,5,3)
168		9524.46	1.33	0.03	0.994(4,6,0) + 0.103(1,7,2)
169	9539.85	9531.82	−3.34	0.00	0.996(4,0,3)
170		9561.57	1.51	0.20	0.978(1,3,4) + 0.199(4,2,2)
171	9631.80	9624.27	2.85	0.04	0.995(1,1,5)
172		9640.77	2.13	0.22	0.998(0,13,0)
173	9667.96	9653.79	1.10	17.31	0.902(0,11,1) + 0.408[0,0,0]
174		9672.77	0.98	0.00	0.999(7,1,0)
175		9697.32	0.13	0.75	0.968(0,9,2) − 0.225(3,8,0)
176	9725.87	9714.10	1.45	2.82	0.941(3,6,1) − 0.273(0,7,3) + 0.163[0,0,0]
177		9717.28	−1.19	0.13	0.974(3,8,0) + 0.223(0,9,2)
178		9732.21	3.69	0.10	0.983(3,4,2) − 0.173(0,5,4)
1	9738.20	9733.50	4.28	59.92	0.773[0,0,0] + 0.482(0,7,3) − 0.383(0,11,1)
179	9747.29	9735.76	−5.73	18.18	0.826(0,7,3) − 0.420[0,0,0] + 0.331(3,6,1) + 0.145(0,11,1)
180	9762.81	9753.87	−3.63	0.04	0.992(3,2,3) − 0.118(0,3,5)
181		9781.28	−1.00	0.45	0.981(0,5,4) + 0.173(3,4,2)
182	9806.85	9796.43	0.19	0.00	0.999(6,1,1)
183		9796.99	−3.81	0.00	0.997(3,0,4)
184	9845.21	9836.87	0.36	0.33	0.989(0,3,5) + 0.118(3,2,3)
185		9856.44	2.00	0.00	1.000(6,3,0)
186		9905.43	−1.05	0.09	0.995(0,1,6)
187		9920.66	0.38	0.25	0.998(2,10,0)
188	9941.20	9928.51	−0.47	1.21	0.993(2,8,1)
189		9950.91	2.18	0.32	0.996(2,6,2)
190	9985.29	9975.53	−4.05	0.18	0.966(2,4,3) − 0.249(5,3,1)
191		9984.01	0.14	0.00	0.989(5,1,2) − 0.139(2,2,4)
192	10 017.80	10 006.31	3.20	0.03	0.968(5,3,1) + 0.248(2,4,3)
193		10 025.87	0.47	0.08	0.988(2,2,4) + 0.139(5,1,2)
194		10 043.60	2.68	0.02	0.999(5,5,0)
195	10 089.66	10 082.40	0.32	0.00	0.998(2,0,5)
196		10 132.64	−0.25	1.19	0.988(1,12,0)
197	10 159.36	10 145.36	−1.82	3.58	0.979(1,10,1) − 0.161[0,1,0]
198		10 174.63	3.75	1.49	0.979(1,8,2) − 0.110(1,12,0)
199		10 185.29	1.81	0.00	0.999(8,0,0)
200	10 209.84	10 198.93	0.70	0.30	0.736(1,6,3) − 0.672(4,5,1)
201		10 203.93	2.02	0.06	0.972(4,3,2) − 0.226(1,4,4)
202	10 222.40	10 213.62	−2.60	0.01	0.981(4,1,3) − 0.114(1,2,5) + 0.112(7,0,1)
203	10 228.12	10 216.13	−0.43	0.39	0.736(4,5,1) + 0.664(1,6,3) − 0.101(4,1,3)
204		10 232.65	0.50	0.13	0.995(4,7,0)
205		10 252.54	1.79	0.33	0.970(1,4,4) + 0.226(4,3,2)
206	10 280.32	10 270.61	−5.37	0.00	0.993(7,0,1) − 0.109(4,1,3)
207	10 312.69	10 304.70	2.39	0.13	0.990(1,2,5) + 0.119(4,1,3)
208		10 352.46	−4.33	8.58	0.919(0,14,0) + 0.285[0,0,1] + 0.235(0,10,2)
209	10 377.37	10 361.78	−3.95	20.26	0.870(0,12,1) − 0.440[0,1,0] − 0.105(1,10,1) + 0.102(0,8,3)
210		10 371.74	3.56	0.00	0.999(7,2,0)
211		10 375.49	5.50	0.01	0.998(1,0,6)
212		10 403.19	8.16	12.35	0.854(0,10,2) − 0.347(0,14,0) + 0.335[0,0,1]
213	10 424.80	10 412.23	−1.97	1.65	0.953(3,7,1) − 0.242(0,8,3) − 0.114(0,12,1) − 0.112[0,1,0]
214		10 415.65	−6.51	0.64	0.947(3,5,2) + 0.246(3,9,0) − 0.166(0,6,4)
215		10 435.48	8.77	2.55	0.945(3,9,0) − 0.254(3,5,2) + 0.157[0,0,1]
216	10 449.22	10 436.67	−1.35	7.30	0.901(0,8,3) − 0.268(0,12,1) − 0.253[0,1,0] + 0.164(3,7,1)
217	10 451.92	10 442.40	−0.95	0.10	0.989(3,3,3) − 0.134(0,4,5)
218		10 446.07	3.59	0.00	0.999(6,0,2)
219		10 477.36	−0.82	0.02	0.994(3,1,4)

TABLE II. (*Continued*.)

No.	Energy (cm^{-1}) $K=N=1$	Energy (cm^{-1}) $K=N=0$	obs.−calc. error (cm^{-1})	$\%A\ ^2B_2$	Eigenvector decomposition
220		10 478.83	1.89	9.79	0.894(0,6,4)+0.303[0,0,1]−0.228(0,10,2)+0.141(3,5,2)− 0.106(3,9,0)
2	10 483.60	10 478.00	−4.02	62.98	0.791[0,1,0]+0.378(0,12,1)+0.318(0,8,3)+0.232(3,7,1)− 0.177(2,9,1)+0.120(1,10,1)−0.102(1,11,1)
221	10 498.19	10 486.38	1.09	0.04	0.999(6,2,1)
3		10 490.20	0.46	59.47	0.768[0,0,1]−0.389(0,6,4)−0.361(0,10,2)−0.182(3,9,0)− 0.151(0,14,0)+0.125(2,11,0)−0.114(3,5,2)
222	10 532.80	10 523.43	−0.29	0.55	0.985(0,4,5)+0.134(3,3,3)
223		10 557.41	2.96	0.01	1.000(6,4,0)
224		10 583.21	1.31	0.25	0.992(0,2,6)
225		10 633.06	−5.47	2.03	0.986(2,11,0)−0.134[0,0,1]
226	10 649.26	10 635.65	−5.56	4.34	0.975(2,9,1)+0.185[0,1,0]
227		10 654.47	7.19	1.98	0.986(2,7,2)−0.105[0,0,1]
228	10 663.43	10 656.54	−3.79	0.02	0.997(0,0,7)
229	10 669.13	10 660.61	−2.00	0.00	0.997(5,0,3)
230	10 677.46	10 667.12	−2.62	0.37	0.965(2,5,3)−0.248(5,4,1)
231		10 670.56	4.17	0.02	0.983(5,2,2)−0.169(2,3,4)
232	10 708.54	10 695.97	0.22	0.08	0.968(5,4,1)+0.246(2,5,3)
233		10 707.27	−0.79	0.17	0.983(2,3,4)+0.168(5,2,2)
234		10 746.09	2.20	0.04	0.999(5,6,0)
235	10 761.97	10 754.37	−0.99	0.03	0.996(2,1,5)
236		10 849.89	−5.27	2.34	0.981(1,13,0)+0.116(1,9,2)−0.113[0,1,1]
237	10 869.80	10 854.53	−14.28	3.57	0.976(1,11,1)+0.124[0,1,0]+0.102[0,2,0]
238		10 876.61	5.09	0.00	0.998(8,1,0)
239		10 879.00	9.70	5.46	0.949(1,9,2)−0.199[0,1,1]−0.148(1,13,0)
240	10 901.50	10 889.80	−2.69	0.88	0.752(1,7,3)−0.627(4,6,1)−0.118(4,2,3)−0.110(1,11,1)
241		10 890.98	2.76	0.12	0.968(4,4,2)−0.241(1,5,4)
242	10 907.11	10 897.58	4.08	0.04	0.971(4,2,3)+0.149(7,1,1)−0.135(1,3,5)
243	10 916.68	10 903.77	−7.24	1.82	0.766(4,6,1)+0.624(1,7,3)
244		10 912.02	−5.64	0.00	0.996(4,0,4)
245		10 928.51	−8.35	0.67	0.862(4,8,0)+0.483(1,5,4)+0.117(4,4,2)
246		10 944.52	5.85	0.41	0.831(1,5,4)−0.498(4,8,0)+0.212(4,4,2)
247	10 964.46	10 952.77	−4.54	0.00	0.987(7,1,1)−0.141(4,2,3)
248	10 990.71	10 981.98	0.62	0.29	0.983(1,3,5)+0.147(4,2,3)
4	11 004.86	10 999.42	1.38	82.75	0.907[1,0,0]−0.331(0,13,1)+0.162(3,8,1)
249		11 041.63	3.55	0.06	0.994(1,1,6)
250		11 063.35	2.72	0.00	0.999(7,3,0)
251		11 070.28	−2.84	25.81	0.636(0,11,2)+0.502(0,15,0)−0.493[0,1,1]−0.167(1,9,2)+ 0.113(0,7,4)
252	b	11 095.50	−14.23	13.89	0.731(0,13,1)+0.514(3,8,1)+0.253[0,2,0]+0.212(0,9,3)+ 0.192[1,0,0]+0.158[0,0,2]
253		11 096.92	4.91	4.83	0.856(0,15,0)−0.426(0,11,2)+0.209[0,1,1]−0.117(3,6,2)
254	11 115.74	11 102.25	−15.83	9.83	0.745(3,8,1)−0.533(0,9,3)−0.259[1,0,0]−0.233(0,13,1) −0.116[0,0,2]
255		11 116.84	5.04	0.60	0.958(3,6,2)−0.181(0,7,4)−0.163(0,11,2)+0.103(3,10,0)
256	11 133.12	11 123.02	−2.67	0.35	0.982(3,4,3)−0.138(0,5,5)
257		11 126.63	10.08	0.00	0.996(6,1,2)
258		11 137.79	4.20	2.21	0.963(3,10,0)−0.153(0,11,2)−0.137[0,1,1]−0.119(3,6,2)
259	11 156.13	11 142.35	9.75	10.02	0.712(0,9,3)−0.500(0,13,1)+0.342(3,8,1)−0.195[1,0,0]+ 0.184[0,2,0]+0.120[0,0,2]
260		11 156.13	3.70	0.06	0.991(3,2,4)−0.109(0,3,6)
261	11 180.48	11 167.17	−2.95	0.02	0.999(6,3,1)
262		11 170.35	1.86	3.03	0.906(0,7,4)−0.308(0,11,2)−0.143(3,10,0)− 0.137[0,1,1]+0.131(3,6,2)
263	11 193.62	11 186.40	−7.36	0.00	0.996(3,0,5)
264	11 216.76	11 206.02	−3.47	22.33	0.862(0,5,5)−0.439[0,2,0]+0.147[0,0,2]+0.129(3,4,3)
5		11 220.93	−0.45	46.44	0.673[0,1,1]+0.480(0,11,2)+0.308(0,7,4)−0.238(2,8,2)+ 0.191(3,10,0)−0.151(2,12,0)+0.141(3,6,2)+0.134(1,9,2)− 0.127(1,10,2)
6	11 218.60	11 210.65	5.99	67.44	0.799[0,2,0]+0.456(0,5,5)−0.239(0,9,3)−0.176[0,0,2]− 0.143(3,8,1)+0.110(2,10,1)
265		11 251.43	0.89	0.02	1.000(6,5,0)
266		11 259.64	3.18	0.53	0.988(0,3,6)+0.109(3,2,4)
7	11 289.51	11 283.15	1.28	73.00	0.848[0,0,2]+0.316(2,10,1)−0.257(0,9,3)+0.165(2,6,3)− 0.113(0,13,1)

TABLE II. (*Continued*.)

No.	Energy (cm^{-1}) $K=N=1$	Energy (cm^{-1}) $K=N=0$	obs.−calc. error (cm^{-1})	$\%A\,^2B_2$	Eigenvector decomposition
267	11 330.12	11 323.62	2.13	0.11	0.994(0,1,7)
268	11 343.61	11 333.99	4.18	0.00	0.976(5,1,3)+0.199(8,0,1)
269		11 346.62	1.68	7.35	0.583(2,8,2)−0.562(5,3,2)−0.559(2,12,0)+0.130(2,4,4)
270	11 363.15	11 348.40	−1.69	6.57	0.872(2,10,1)−0.393(2,6,3)−0.197[0,0,2]−0.128[0,2,0]
271		11 354.63	9.79	0.47	0.801(5,3,2)+0.413(2,8,2)−0.398(2,12,0)−0.138(2,4,4)
272		11 363.15	3.86	0.00	0.997(9,0,0)
273	11 392.43	11 381.46	21.95	8.50	0.856(2,6,3)+0.318(2,10,1)−0.264(5,5,1)−0.250[0,0,2] −0.109[0,2,0]
274		11 376.48	18.41	0.97	0.707(2,12,0)+0.632(2,8,2)+0.249[0,1,1]+0.100(0,11,2)
275	b	11 379.42	−5.62	0.60	0.961(5,5,1)+0.262(2,6,3)
276		11 381.20	−6.30	0.41	0.977(2,4,4)+0.187(5,3,2)
277	11 410.73	11 400.23	−12.14	0.00	0.976(8,0,1)−0.191(5,1,3)+0.106(2,2,5)
278	11 430.99	11 422.84	−3.51	0.10	0.988(2,2,5)
279		11 440.67	−2.05	0.15	0.998(5,7,0)
280		11 477.76	−2.35	0.00	0.997(2,0,6)
281		11 547.93	2.07	0.00	0.970(7,0,2)+0.242(4,1,4)
282	b	11 553.37	−13.81	0.13	0.969(4,3,3)+0.176(7,2,1)−0.152(1,4,5)
283		11 557.04	1.70	0.00	0.997(8,2,0)
284		11 570.90	0.98	0.50	0.957(4,5,2)−0.257(1,6,4)
285		11 576.34	9.45	2.16	0.917(1,14,0)−0.351(1,10,2)−0.100[0,2,1]
286		11 593.63	3.85	7.02	0.867(1,10,2)+0.362(1,14,0)+0.186[0,2,1]−0.185(4,9,0) +0.167[0,1,1]
287	11 580.82	11 568.20	−13.09	3.26	0.741(1,8,3)−0.602(4,7,1)−0.210(1,12,1)−0.115[0,1,2]
288	11 591.20	11 574.30	−1.35	4.89	0.943(1,12,1)−0.233(4,7,1)+0.127[1,1,0]−0.104[0,0,2]
289		11 601.89	15.66	0.01	0.963(4,1,4)−0.242(7,0,2)
290	b	11 604.43	4.18	6.86	0.731(4,7,1)+0.599(1,8,3)−0.161[1,1,0]+0.153(1,12,1) −0.146[0,1,2]−0.101[0,0,2]
291		11 619.38	−0.86	2.26	0.941(1,6,4)+0.245(4,5,2)
292	11 638.61	11 624.79	−9.21	0.01	0.981(7,2,1)−0.161(4,3,3)+0.104(1,4,5)
293		11 635.86	−1.77	2.75	0.961(4,9,0)+0.171(1,10,2)+0.149[1,0,1]
294	11 664.04	11 654.32	−3.21	0.63	0.973(1,4,5)+0.167(4,3,3)
8		11 694.41	0.97	71.40	0.841[1,1,0]+0.319(0,14,1)−0.274(3,9,1)+0.197(4,7,1) +0.126(0,10,3)
295		11 704.48	−0.20	0.21	0.990(1,2,6)+0.101(4,1,4)
9		11 720.41	a	60.6	0.771[1,0,1]−0.349(0,12,2)−0.292(0,16,0)+0.243(3,7,2) +0.180(3,11,0)−0.180(4,9,0)
296		11 742.84	−6.09	0.01	0.999(7,4,0)
297	11 768.58	11 759.14	8.15	0.00	0.999(6,0,3)
298	11 783.85	11 776.96	7.96	0.01	0.997(1,0,7)

[a]Calculated frequency.
[b]$K=N=0$ limit deduced from $K=0$, $N=1,3,5,...$ LIF, ICLAS or CRDS experimental energies.

shifts discussed in the paragraph above. Interestingly, one however also observes a certain number of interactions between two states of the ground electronic surface, which are coupled by non-negligible $\langle \psi_m^g|\mathbf{H}|\psi_n^g\rangle$ matrix elements [see Eq. (3.6)]. Nonetheless, due the much smaller value for λ (332 cm^{-1} against more than 2400 cm^{-1}), the mixing coefficients reported in the two last columns of Table II remain much smaller than those obtained by Leonardi and Petrongolo.[11]

V. CONCLUSION

We have derived an efficient method for adjusting the parameters of an effective Hamiltonian against experimental data. This model accurately reproduces the observed frequencies up to a few thousands of cm^{-1} above the conical intersection. Continuation of this work is expected in two directions. First, we plan to use the effective Hamiltonian derived in this article to reproduce the absorption spectra, which have been recorded by the ICLAS and FTS techniques in the range 11 200–16 150 cm^{-1}.[2,17] While the goal would, of course, no longer be to calculate all transition energies with an error of the order of a few cm^{-1}, a visual or statistical comparison of the observed and calculated spectra should be able to indicate up to what energies such a model remains valid, and eventually what corrections are needed. Moreover, we plan to analyze the classical phase space of the vibronically coupled system along the lines proposed in Refs. 18 and 19. The underlying idea is to use the classical periodic orbits of the system to study the nonadiabatic quantum dynamics, as was done recently for several triatomic molecules in the context of the Born–Oppenheimer approximation (see, for example, Refs. 20 and 21, and references therein).

APPENDIX: CALCULATION OF THE $\langle v_1', v_2', v_3' | q_3^n | v_1, v_2, v_3 \rangle$ INTEGRALS

Since, for symmetry reasons, the matrix $\mathbf{A}=\{A_{jk}\}$ is block diagonal [cf. Eq. (2.6)], the integrals to compute split in the more manageable form,

$$\langle v_1', v_2', v_3' | q_3^n | v_1, v_2, v_3 \rangle = \langle v_1', v_2' | v_1, v_2 \rangle \langle v_3' | q_3^n | v_3 \rangle. \tag{A1}$$

After some straightforward algebra, the second integral in the right-hand side of Eq. (A1) is rewritten as

$$\langle v_3' | q_3^n | v_3 \rangle = C_3(n, v_3, v_3') \times \int_{-\infty}^{+\infty} P_3(n, v_3, v_3' | x_3) e^{-x_3^2} dx_3, \tag{A2}$$

where

$$\begin{aligned} \alpha_3 &= \sqrt{\frac{2}{1+A_{33}^2}}, \\ C_3(n, v_3, v_3') &= \alpha_3^{1+n} \sqrt{\frac{A_{33}}{\pi v_3! v_3' ! 2^{v_3+v_3'}}}, \\ q_3 &= \alpha_3 x_3, \\ P_3(n, v_3, v_3' | x_3) &= x_3^n H_{v_3}(\alpha_3 x_3) H_{v_3'}(A_{33}\alpha_3 x_3), \end{aligned} \tag{A3}$$

and the H_m's are the Hermite polynomials of order m. The polynomial $P_3(n, v_3, v_3' | x_3)$ is next projected on the orthogonal basis of the Hermite polynomials, leading to

$$P_3(n, v_3, v_3' | x_3) = \sum_{k=0}^{n+v_3+v_3'} a_3(n, v_3, v_3' | k) H_k(x_3). \tag{A4}$$

Remembering that the term of $H_k(x)$ with highest order is $2^k x^k$, the real coefficients $a_3(n, v_3, v_3' | k)$ are easily obtained downwards, starting with $a_3(n, v_3, v_3' | n+v_3+v_3')$ and ending with $a_3(n, v_3, v_3' | 0)$. The second integral in the right-hand side of Eq. (A1) is then just

$$\langle v_3' | q_3^n | v_3 \rangle = \sqrt{\pi} C_3(n, v_3, v_3') a_3(n, v_3, v_3' | 0). \tag{A5}$$

Calculation of the first integral in the right-hand side of Eq. (A1) is somewhat more tedious, but this can again be performed without ever integrating a function numerically, which is of fundamental importance for the sake of accuracy. Proceeding along the same lines as in Refs. 4 and 22, one first obtains, by inverting Eq. (2.6), the matrices $\mathbf{T}$ and $\mathbf{D}$, such that

$$\begin{pmatrix} q_1 \\ q_2 \end{pmatrix} = \mathbf{T} \begin{pmatrix} q_1' \\ q_2' \end{pmatrix} + \mathbf{D}. \tag{A6}$$

One then calculates the orthogonal matrix $\mathbf{W}$ and the diagonal matrix $\mathbf{G}$ of, respectively, the eigenvectors and eigenvalues of ${}^t\mathbf{T}\,\mathbf{T}$,

$${}^t\mathbf{T}\ \mathbf{T}\ \mathbf{W} = \mathbf{W}\ \mathbf{G}. \tag{A7}$$

The matrix $\mathbf{U}$ and the vectors $\mathbf{d}$ and $\mathbf{s}$ are defined from $\mathbf{W}$ and $\mathbf{G}$ according to

$$\begin{aligned} \mathbf{U} &= \mathbf{T}\ \mathbf{W}, \\ \mathbf{d} &= \mathbf{G}^{1/2}\mathbf{U}^{-1}\mathbf{D}, \\ \mathbf{s} &= \begin{pmatrix} s_1 \\ s_2 \end{pmatrix} = \mathbf{W}^{-1} \begin{pmatrix} q_1' \\ q_2' \end{pmatrix}. \end{aligned} \tag{A8}$$

One finally notes

$$\begin{aligned} \alpha_j &= \sqrt{\frac{2}{1+G_{jj}}}, \\ \beta_j &= \frac{d_j \sqrt{G_{jj}}}{1+G_{jj}}, \\ \gamma_j &= \frac{d_j^2}{2(1+G_{jj})}, \\ s_j &= \alpha_j x_j - \beta_j \end{aligned} \tag{A9}$$

($j=1,2$). After some straightforward algebra, whose first steps are sketched in Refs. 4 and 22, the first integral in the right-hand side of Eq. (A1) is recast in the form,

$$\begin{aligned} \langle v_1', v_2' | v_1, v_2 \rangle = {} & C(v_1, v_2, v_1', v_2') \\ & \times \sum_{i_1=0}^{v_1} \sum_{i_2=0}^{v_2} \sum_{i_1'=0}^{v_1'} \sum_{i_2'=0}^{v_2'} \binom{v_1}{i_1} \binom{v_2}{i_2} \binom{v_1'}{i_1'} \binom{v_2'}{i_2'} \\ & \times \int_{-\infty}^{+\infty} P_1(i_1, i_2, i_1', i_2' | x_1) e^{-x_1^2} dx_1 \\ & \times \int_{-\infty}^{+\infty} P_2(v_1 - i_1, v_2 - i_2, v_1' - i_1', v_2' \\ & - i_2' | x_2) e^{-x_2^2} dx_2, \end{aligned} \tag{A10}$$

where

$$\begin{aligned} C(v_1, v_2, v_1', v_2') &= \frac{\alpha_1 \alpha_2 e^{-\gamma_1 - \gamma_2} \det(\mathbf{W})}{\pi 2^{v_1+v_2+v_1'+v_2'}} \sqrt{\frac{\det(\mathbf{T})}{v_1! v_2! v_1'! v_2'!}}, \\ P_1(i_1, i_2, i_1', i_2' | x_1) &= H_{i_1}(\sqrt{2}(U_{11}s_1 + D_1)) H_{i_2}(\sqrt{2} U_{21} s_1) \\ &\quad \times H_{i_1'}(\sqrt{2} W_{11} s_1) H_{i_2'}(\sqrt{2} W_{21} s_1), \end{aligned} \tag{A11}$$

$$\begin{aligned} P_2(i_1, i_2, i_1', i_2' | x_2) &= H_{i_1}(\sqrt{2} U_{12} s_2) H_{i_2}(\sqrt{2}(U_{22}s_2 + D_2)) \\ &\quad \times H_{i_1'}(\sqrt{2} W_{12} s_2) H_{i_2'}(\sqrt{2} W_{22} s_2), \end{aligned}$$

and the s_j's must be replaced with their expressions in terms of the x_j's in Eq. (A9). As for the integral dealing with mode 3, each polynomial $P_j(i_1, i_2, i_1', i_2' | x_j)$ ($j=1,2$) is next projected on the orthogonal basis of the Hermite polynomials, according to

$$P_j(i_1, i_2, i_1', i_2' | x_j) = \sum_{k=0}^{i_1+i_2+i_1'+i_2'} a_j(i_1, i_2, i_1', i_2' | k) H_k(x_j), \tag{A12}$$

so that the corresponding integrals are equal to

$$\int_{-\infty}^{+\infty} P_j(i_1, i_2, i_1', i_2' | x_j) e^{-x_j^2} dx_j = \sqrt{\pi} a_j(i_1, i_2, i_1', i_2' | 0) \tag{A13}$$

($j=1,2$). It is stressed, that the number of accuracy digits, which are lost when computing the real coefficients a_j and the quadruple sum in Eq. (A10), is sometimes larger than 50 for the $\langle v_1',v_2',v_3'|q_3^n|v_1,v_2,v_3\rangle$ integrals used in this work. Therefore, one has to evaluate these integrals with packages, which allow for arbitrarily large numbers of working digits, and to check that the number of significant digits at the end of the calculations is still large enough.

[1] A. Delon and R. Jost, J. Chem. Phys. **95**, 5686 (1991).
[2] R. Georges, A. Delon, F. Bylicki, R. Jost, A. Campargue, A. Charvat, M. Chenevier, and F. Stoeckel, Chem. Phys. **190**, 207 (1995).
[3] B. Kirmse, A. Delon, and R. Jost, J. Chem. Phys. **108**, 6638 (1998).
[4] A. Delon, R. Jost, and M. Jacon, J. Chem. Phys. **114**, 331 (2001).
[5] A. Delon, R. Jost, and M. Lombardi, J. Chem. Phys. **95**, 5701 (1991).
[6] E. Haller, H. Köppel, and L. S. Cederbaum, J. Mol. Spectrosc. **111**, 377 (1985).
[7] S. Mahapatra, H. Köppel, and L. S. Cederbaum, J. Chem. Phys. **110**, 5691 (1999).
[8] S. Mahapatra, H. Köppel, L. S. Cederbaum, P. Stampfuss, and W. Wenzel, Chem. Phys. **259**, 211 (2000).
[9] R. F. Salzgeber, V. A. Mandelshtam, Ch. Schlier, and H. S. Taylor, J. Chem. Phys. **110**, 3756 (1999).
[10] E. Leonardi, C. Petrongolo, G. Hirsch, and R. J. Buenker, J. Chem. Phys. **105**, 9051 (1996).
[11] E. Leonardi and C. Petrongolo, J. Chem. Phys. **106**, 10066 (1997).
[12] R. Brandi, F. Santoro, and C. Petrongolo, Chem. Phys. **225**, 55 (1997).
[13] F. Santoro and C. Petrongolo, J. Chem. Phys. **110**, 4419 (1999).
[14] R. Jost, M. Joyeux, and M. Jacon, Chem. Phys. **283**, 17 (2002).
[15] D. Sugny and M. Joyeux, Chem. Phys. Lett. **337**, 319 (2001).
[16] M. Joyeux, D. Sugny, and M. Lombardi, Chem. Phys. Lett. **352**, 99 (2002).
[17] J. Orphal, S. Dreher, S. Voigt, J. P. Burrows, R. Jost, and A. Delon, J. Chem. Phys. **109**, 10217 (1998).
[18] S. Dilthey and G. Stock, Phys. Rev. Lett. **87**, 140404 (2001).
[19] S. Dilthey, B. Mehlig, and G. Stock, J. Chem. Phys. **116**, 69 (2002).
[20] H. Ishikawa, R. W. Field, S. C. Farantos, M. Joyeux, J. Koput, C. Beck, and R. Schinke, Annu. Rev. Phys. Chem. **50**, 443 (1999).
[21] M. Joyeux, S. C. Farantos, and R. Schinke, J. Phys. Chem. A **106**, 5407 (2002).
[22] T. R. Faulkner and F. S. Richardson, J. Chem. Phys. **70**, 1201 (1979).